UNIVERSITY OF OKLAHOMA

GRADUATE COLLEGE

EFFECT OF ALIGNMENT ON THERMAL CONDUCTIVITY OF POLYETHYLENE-GRAPHENE COMPOSITES AND COMPARISON WITH EFFECTIVE MEDIUM THEORY

A THESIS

SUBMITTED TO THE GRADUATE FACULTY

in partial fulfillment of the requirements for the

Degree of

MASTER OF SCIENCE

By

FATEMA TARANNUM
Norman, Oklahoma
2019

EFFECT OF ALIGNMENT ON THERMAL CONDUCTIVITY OF POLYETHYLENE-GRAPHENE COMPOSITES AND COMPARISON WITH EFFECTIVE MEDIUM THEORY

A THESIS APPROVED FOR THE SCHOOL OF AEROSPACE AND MECHANICAL ENGINEERING

BY

Dr. Jivtesh Garg, Chair

Dr. M. Cengiz Altan

Dr. Yingtao Liu

Acknowledgements

I feel blessed for being able to successfully achieve my Master of Science at the University of Oklahoma and I would like to thank my adviser and committee chair, Dr. Jivtesh Garg for the academic support, time, patience. Also, I would like to thank Professor M. Cengiz Altan and Dr. Yantao Li, my other committee members for their valuable comments to ensure that I executed the work in a way that made sense for everyone. I especially would like to thank Professor Brian Grady for allowing me to access his laboratory equipment. I am thankful to Dr. Tingting Gu for her guidance and assistance for the image analysis using Leica SP8 Laser Scanning Confocal Microscopy. I would like to acknowledge and thank the School of Aerospace and Mechanical Engineering staff for their support. Finally, I am very grateful to my family and friends especially my mother, Hosne Ara Begum and my sister, Morium Tabassum for their encouragement and support throughout this process.

Table of Contents

List of Tables

List of Figures

Abstract

Polymers show low thermal conductivity (<0.5 W/mK) in comparison to metals (>20 W/mK). Increased thermal conductivity of polymers can lead to useful applications in industry. The main objective of this research is to analyze the effect of alignment of polymer lamellae and graphene nanoplatelets on thermal conductivity enhancement of polymer-graphene nanocomposites. Role of increase of graphene content in polyethylene-graphene nanoplatelet (PE-GNP) composite materials is also studied.

A twin conical screw micro compounder is used to prepare PE-GNP composites with 9 weight% and 13 weight% graphene nanoplatelet. Linear mechanical stretching is used to achieve alignment of polymer and graphene. Thermal conductivity of nanocomposite samples is measured using Angstrom Method. To analyze the alignment of GNP flakes, Laser Scanning Confocal Microscopy (LSCM) is used. Effective medium theory (EMT) is used to compare predicted and measured thermal conductivity values. Thermal conductivity, *k* values obtained from EMT model indicate an agreement with experimentally measured values for 9 weight% and 13 weight% GNP content in the composite.

Chapter 1: Introduction

1.1 Motivation

Rapid developments in the processing and synthesis of carbon-based nanomaterials have created new avenues to achieve high thermal conductivity materials in the last two decades. The power required for some processor modules can reach 250W in a high-performance computer [1]. Prompt heat dissipation is very necessary for extended lifetime and efficiency of the system. High thermal conductivity materials are strongly recommended to eradicate this thermal issue and enhance the performance of thermal management system[2].

The operating limitations of metallic heat exchangers in some applications have created the need of using polymers because of their resistance to fouling and corrosion. Use of polymers offers substantial weight, volume, space, and cost savings which can provide a competitive edge over heat exchangers manufactured from more exotic metallic alloys [3]. Moreover, the energy required to produce polymers is about two times lower than common metals, making them environmentally attractive. Polymers, due to their resistance to chemicals, also improve reliability in corrosive environments such as natural gas liquefaction in offshore applications and condensing boilers where they hold potential to replace expensive metals such as titanium [4-6]. Heat exchangers[7, 8] based on polymers such as polyethylene and polypropylene are extensively used in various fields including water desalination [9], solar energy harvesting [10], automotive control units [11] and micro-electronics cooling [12-14].

Polymers have also been commonly used as aerospace materials and electronics packaging materials because of their various excellent properties[15, 16]. Polymers, however, typically have quite low thermal conductivity (~0.1-0.5 W/m K) [3, 17] due to random orientation of polymer

lamellae and presence of amorphous regions as shown in Figure 1.1. Some representative values are presented in Table 1.1. Most of the heat in polymers is conducted by phonons which are quantized modes of vibration in a crystal lattice [18].

Table 1.1. Material Thermal Conductivity at 25°C (W/m K) [3, 17, 19]

Material	Thermal Conductivity ($Wm^{-1}K^{-1}$)
Low density polyethylene (LDPE)	0.30
High density polyethylene (HDPE)	0.44
Polypropylene (PP)	0.11
Polystyrene (PS)	0.14
Polymethylmethacrylate (PMMA)	0.21
Nylon-6 (PA6)	0.25
Nylon-6.6 (PA66)	0.26
Poly(ethylene terephthalate) (PET)	0.15

Composite materials are typically more desirable than traditional materials due to their enhanced properties [20]. Different nanocomposite-based systems can be processed by combining different polymers and fillers at the nanoscale level. High thermal conductivity materials are used as fillers to enhance the thermal conductivity of polymer matrix [21-28]. Metallic fillers have been widely used in polymer composites to improve their thermal conductivity[29]. The thermal conductivity of metallic fillers can reach and exceed 100 $Wm^{-1}K^{-1}$[30]. Nanomaterials such as graphene have excellent thermal conductivity (exceeding 1000 W/mK) and can lead to polymer composites with enhanced thermal properties [31].

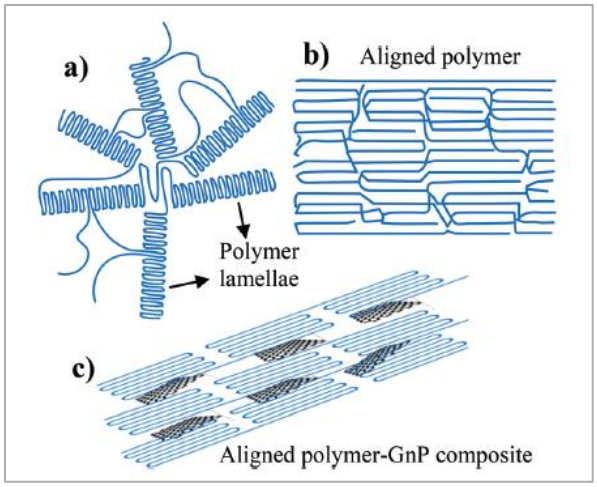

Figure 1.1. (a) Randomly oriented polymer lamellae in a semi-crystalline polymer, (b) alignment induced by strain and (c) aligned polymer-GnP composite [6]

In this work, polyethylene (PE) is used as the polymer matrix and graphene nanoplatelets are used as nano filler material because of their superior thermal conductivity of 1500-5000 $Wm^{-1}K^{-1}$[6, 32-34]. Fig. 1.1(a) shows a typical structure of a semi-crystalline polyethylene, which consists of crystalline domains (called lamellae) where polymer chains are aligned periodically, and amorphous domains where the polymer chains are randomly entangled [35]. The low thermal conductivity of polymers, on the order of 0.1-0.5 $Wm^{-1}K^{-1}$, is due to the disordered amorphous region and random orientation of lamellae. By drawing polyethylene into highly aligned fibers, chain entanglements, which act as phonon scattering centers, are significantly reduced, leading to a thermal conductivity increase by ~2 orders of magnitude [36-38].

Polymer-graphene nanocomposites can be synthesized by several methods, such as solution blending, melt mixing, and in-situ polymerization [39-41]. Graphene has very high in-plane thermal conductivity (~1500 – 5000 $Wm^{-1}K^{-1}$) but low out-of-plane value (~10 $Wm^{-1}K^{-1}$). Due to this, random orientation of GNPs limits their contribution to thermal conductivity enhancement along a given direction. Alignment of both the polymer lamellae and GNPs along a given direction

(Figure 1.1) can cause high thermal conductivity values along that direction. Several studies have addressed alignment effects. Different approaches like mechanical stretching [42], electric field [43-48] and magnetic field [49-51] can be used for orientation of nanofillers. Mechanical stretching has been used for alignment of both the polymer matrix [52, 53] and dispersed filler material [54, 55]. Shen *et al.* achieved high thermal conductivity of 104 $Wm^{-1}K^{-1}$ for polyethylene (PE) after using a two-stage heating method to stretch the nanofibers up to 400 draw ratio[35, 56]. Choy *et al.* [57-59], found that the thermal conductivity of ultrahigh molecular weight polyethylene (UHMW-PE) could exceed 40 $Wm^{-1}K^{-1}$ when the draw ratio reaches beyond 300 [59]. In another report, the effect of the alignment of polymer chains was used to achieve a thermal conductivity of ~16 $Wm^{-1}K^{-1}$ in polyethylene films at draw ratios approaching ~100 [60].

Amy *et al.* reported thermal conductivity of aligned multiwall CNT nanocomposite films for different volume fractions of CNT. Dense aligned arrays of 17 vol % CNTs enhanced the thermal conductivity by a factor of 18 [61]. According to Yan *et al.* magnetic field in the epoxy composites was used to align magnetic GnP–Fe_3O_4 hybrids. It was found that homogeneous, aligned GnP–Fe_3O_4 hybrids enhance *k* value of epoxy almost by 40% in comparison with randomly oriented GnPs in the composite [51, 60]. Sihn *et al.* used aligned CNTs in adhesively bonded joints to achieve higher through-thickness thermal conductivity. The value of through thick thermal conductivity was over 250 W/mK^{-1}, which ultimately supersedes the thermal conductivity of sample with neat adhesive joint[62]. Song *et al.* used self-alignment method and found thermal conductivity of 6.168 $Wm^{-1}K^{-1}$ for nanofibrillated cellulose (NFC) and in situ reduced graphene oxide (RGO) nanosheets hybrid film[63]. For GNP/PDMS (polydimethylsiloxane) composite Guo *et al.* reached at 6.05 $Wm^{-1}K^{-1}$ for 20vol% GNP aligned using electric field method [64].

1.2 Research Objective

Inspired by the different experiments on the alignment effect of nanofiller polymer composites, the effect of simultaneous alignment on thermal property of GNP filler-based polyethylene nanocomposites has been carried out through this study. Thermal conductivity enhancement through aligning both the graphene nanoplatelet and the polymer matrix simultaneously is the main objective of this experimental analysis.

Chapter 2: Materials and Preparation Method

Polymer composites are obtained by combining a natural or synthetic filler with the polymer matrix. Matrix, filler, and interface properties and microstructure are the main factors that determine the properties of composite materials. In a composite material, the matrix is used as the dispersion medium (continuous phase) for the dispersed or filler material. In this work, graphene nanoplatelets are dispersed in the polymer matrix which is chosen to be high density polyethylene. All the experiments are performed using 9wt% and 13wt% of graphene nanoplatelets. A description of materials and processing methods is provided below.

2.1 Materials

2.1.1 High Density Polyethylene

High density polyethylene (HDPE) is a linear, semi-crystalline homopolymer of ethylene. Because of low degree of branching, it has high density. Chemical formula of the polymer is $H(CH_2CH_2)_nH$ where n is the number of basic repeating units. The properties of high-density polyethylene used for this experiment are presented in table 2.1

Table 2.1. High density polyethylene properties (from Sigma-Aldrich) [6]

Melt Index	2.2 g/10 min (190 °C/2.16kg)
Hardness	65 (Shore D, ASTM D 2240)
Transition temperature	Softening point 123 °C (Vicat, ASTM D 1525)
Density	0.93-0.97 (g/cm^3)

2.1.2 Specific Heat and Density Measurement of High-Density Polyethylene

Pycnometer (AccuPyc 1340V2.0) is used to measure the density and Differential Scanning Calorimetry (DSC) technique is used to measure specific heat of the pure high-density polyethylene specimen. Table 2.2 presents the specific heat analysis of pure polyethylene respectively. The density of polyethylene is measured to be 0.98g/cm^3.

Table 2.2: Specific Heat Analysis of High-Density Polyethylene [53]

Temperature (℃)	Specific Heat (J/g℃)
0	2.0
6.85	2.0
16.85	2.1
26.85	2.1
36.85	2.2
46.85	2.4
56.85	2.5

2.1.3 Graphene

Graphene, or mono-layer graphite, is a single-atom-thick sheet of 2-D bonded carbon atoms which are tightly packed in a hexagonal crystalline structure with over 100-fold anisotropy of heat flow between the in-plane and out-of-plane directions [65]. Graphene is naturally referred to as a single layer of graphite, but also exist as bilayer or trilayer graphene. Due to the lattice arrangement, edges of graphene can be either armchair or a zig-zag edge [66].

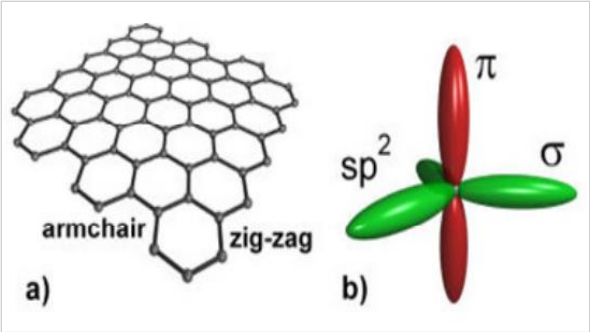

Figure 2.1. a) Armchair and zig-zag edges in graphene, b) sp^2 hybridization illustrated in graphene [66]

The possibility of wrapping up graphene into 0D fullerenes, rolling it into 1D carbon nanotubes (CNTs) and stacking of it into 3D graphite makes graphene the central building block of all graphitic materials (see Figure 2.2) [67, 68].

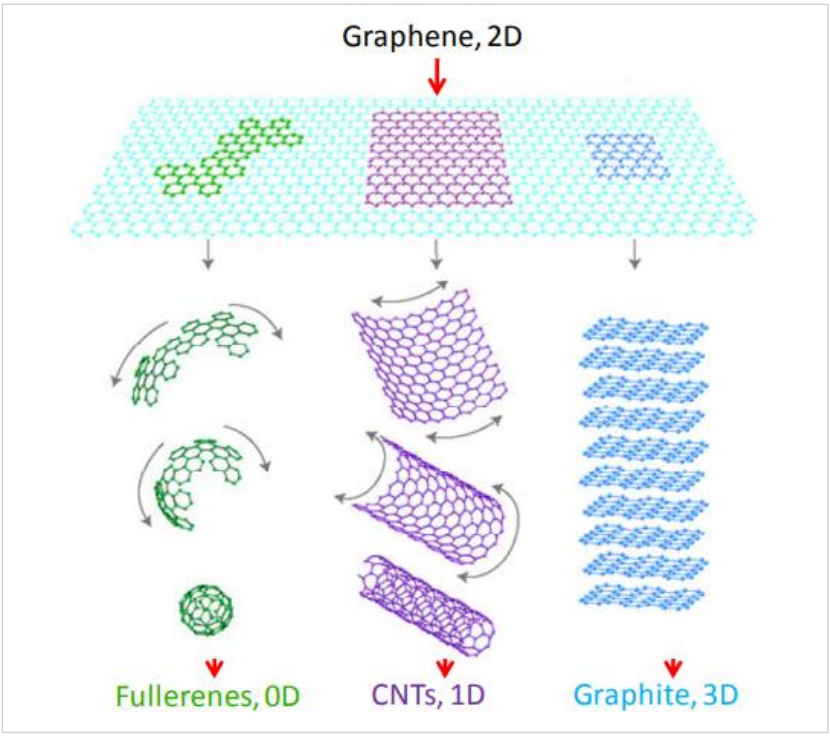

Figure 2.2. Carbon materials as fullerenes, carbon nanotubes (CNTs) and graphite (0D, 1D and 3D respectively) can be derived from single layer graphene (2D) [67]

Carbon atoms have a total of 6 electrons where 2 remain in the inner shell and other 4 remain in the outer shell. These 4 outer shell electrons of an individual carbon atom displays the availability for chemical bonding. But each atom is connected to 3 other carbon atoms on the two-dimensional plane in graphene. Along with this, it leaves 1 electron freely available in the third dimension for electronic conduction. These highly mobile electrons called pi (π) electrons which are located above and below the graphene sheet. These overlapping pi orbitals help to enhance carbon to carbon bonds in graphene. This strong and anisotropic bonding with the low mass of the carbon atoms give graphene its unique thermal properties. Eventually, the unusual thermal properties of graphene comes from its 2D nature, which leads it to ideal thermal management applications [69].

Nika *et al.* [70] and Kong *et al.* [71] found thermal conductivity values of graphene in the range of 2000–6000 $Wm^{-1}K^{-1}$ using first principle calculations. Fugallo *et al.* [33] also used first-principles transport calculations and predicted that the highest *k* value is 3600 $Wm^{-1}K^{-1}$for natural graphene and 4300 $Wm^{-1}K^{-1}$ for isotopic pure graphene at room temperature. Baladin *et al.* has reported *k* value of 5300 $Wm^{-1}K^{-1}$ for partially suspended graphene sheet at room temperature[72]. Balandin [73] also demonstrated that in-plane thermal conductivity of graphene at room temperature is about 2000–4000 $Wm^{-1}K^{-1}$for freely suspended samples. Other experiments suggest graphene has thermal conductivity of 3000–5000 $Wm^{-1}K^{-1}$ for a length of ~10 μm[74].

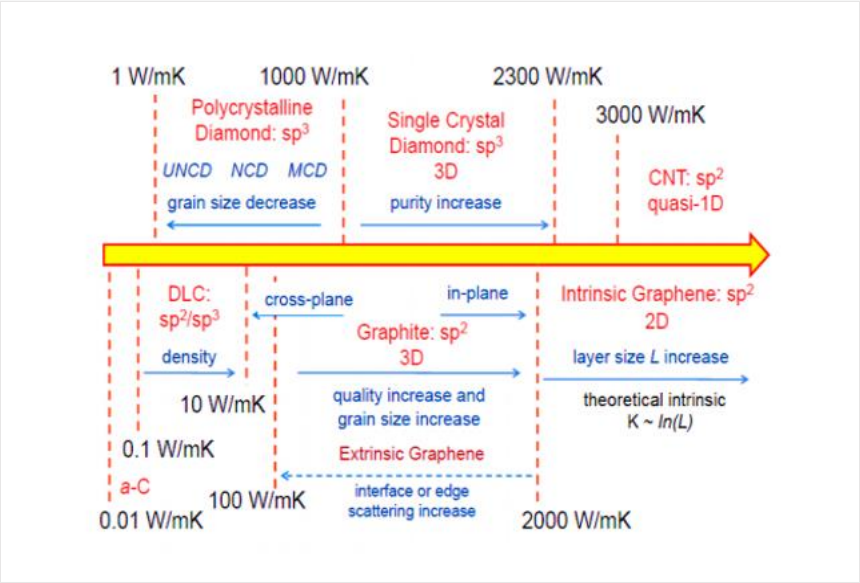

Figure 2.3. Thermal properties of carbon allotropes and derivatives [73]

2.1.4 Graphene Nanoplatelet

Graphene nanoplatelets (GNPs) have drawn a lot of interest due to their electrical conductivity and mechanical properties where the in-plane thermal conductivity of GNPs is stated as 3,000 to 5,000 $Wm^{-1}K^{-1}$ [32, 75].

Graphene nanoplatelets have an average thickness of 5 to10 nm and a specific surface area of 50 to 750 m^2/g; they can be produced at different lateral sizes, from 1 to 50μm. These kind of nanoparticles, include short stacks of platelet-shaped graphene sheets, and are identical to those found in the walls of carbon nanotubes but in planar form [76].

Highest quality graphene with minimal defect density has been used for this study to facilitate achievement of high thermal conductivities. In this experimental work, the flakes have very low defect density due to being produced directly by mechanical exfoliation from raw graphite. Table 2.3 presents the properties of graphene flakes used in this study.

Table 2.3. Specifications of GNP flakes available at Graphene Supermarket [6]

Average flake thickness	60 nm
Specific surface area	<15m^2
Particle (lateral) size	~ 3-7 μm

2.2 Processes Involved

2.2.1 Melt Mixing

There are several ways for dispersing nanofillers in polymer matrices, including in situ polymerization and melting or solution mixing. The melt mixing consists of dispersing the nanoparticles by mechanical shearing action in the polymer matrix in the molten state. The solution mixing involves dispersion of nanoparticles in a solution containing the solubilized polymer matrix. Due to the low solution viscosity, the method tends to facilitate better dispersion of nanoparticles in the polymer matrix compared to melt mixing [77]. In this work, we used melt mixing to prepare the composites.

2.2.1 Micro-compounding

The PE-GNP nanocomposites in this work were prepared by using a DSM Xplore 5 cc micro-compounder by melting polyethylene pellets inside the chamber of the micro compounder and mixing the molten polymer with graphene nanoplatelets. DSM Xplore 5 cc micro-compounder enables good control over the microstructure of the composite through control of parameters such as mixing time, temperature and screw rotation speed.

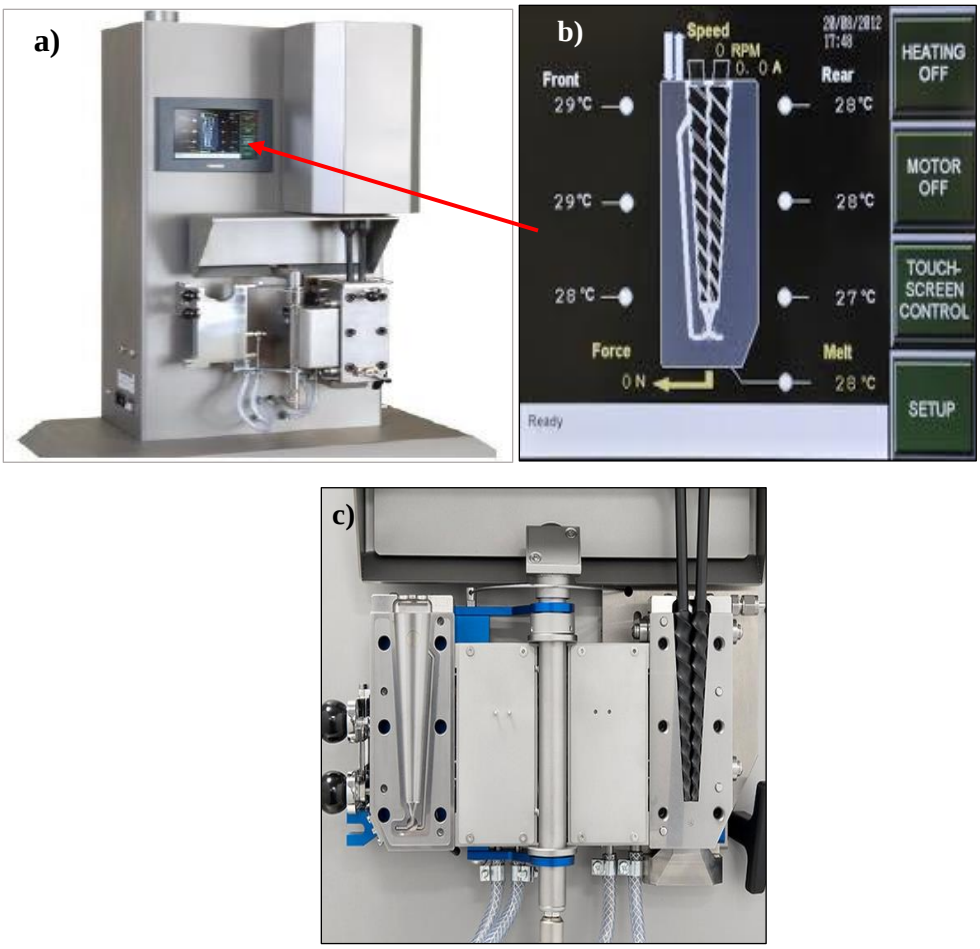

Figure 2.4. a) DSM Xplore 5 cc Micro-Compounder, b) Temperature controlled section, c) Chamber with conical screw

Rotation of two conical mixing screws inside the sealed chamber showed in figure 2.4, during the mixing process, facilitates good dispersion of the nanoplatelets through application of high shear forces.

Mixing time, temperature and speed are the main factors that determine dispersion of GNPs in the polymer matrix. Longer mixing time can provide better dispersion, however it can also damage the nanoplatelets. Mixing time is chosen to be between 40 to 90 minutes. Higher speed of screws and temperature can also cause damage the composite. On the other hand, lower temperature, mixing time and speed may prevent uniform dispersion of GnPs. Due to these considerations, mixing temperatures of 160°C to 220°C and rotation speed of 200-220 rpm is chosen in this work.

2.2.2 Compression Molding

Figure 2.5: Carver hot press for compression molding.

After the dispersion of GNP filler in the polymer matrix, the material is taken out from the mixing chamber of the micro-compounder. Then, carver hot press is used for compression-molding of the blended composite. A pressure of 1 MPa pressure along with a temperature of 145 °C is used for 15 min. Approximately 1-mm-thick specimens are fabricated. The pressure is sustained while the specimen is allowed to cool down gradually to the ambient temperature (typically, 23 °C) at a typical rate of 2.5 °C/min.

2.2.3 Mechanical Stretching

To achieve alignment, mechanical stretching is used. Sample is fixed on linear motorized sliding machine to achieve mechanical stretching. The motor driven machine has the capability of applying 100lb of force.

Lower extension rates are chosen to avoid sample failure during stretching and also achieve uniform stretching throughout the length of the composite sample. Heat is further applied to also

facilitate sample stretching. Upon stretching, different draw ratios (ratio of length after stretching to the original length of sample) can be achieved for each sample.

Figure 2.6. a) Unstretched PE-GNP specimen with draw ratio of 1, b) Stretched PE-GNP specimen with draw ratio of 5

Chapter 3: Thermal Conductivity Measurement

Many methods have been proposed and used for measurement of thermal conductivity. Static methods involve measurements of the temperature gradient in conjunction with an applied heat flux. Dynamic methods are typically more effective at room temperature, heat losses having a smaller effect on the measurement [78]. In this work we use a dynamic method developed by Ångström in 1863 [79, 80]. The method is described below.

3.1 Ångström Method

The thermal conductivity (k) can be obtained from specific heat (C_p), density (ρ), and thermal diffusivity(α) using $k = \alpha\rho C_p$.

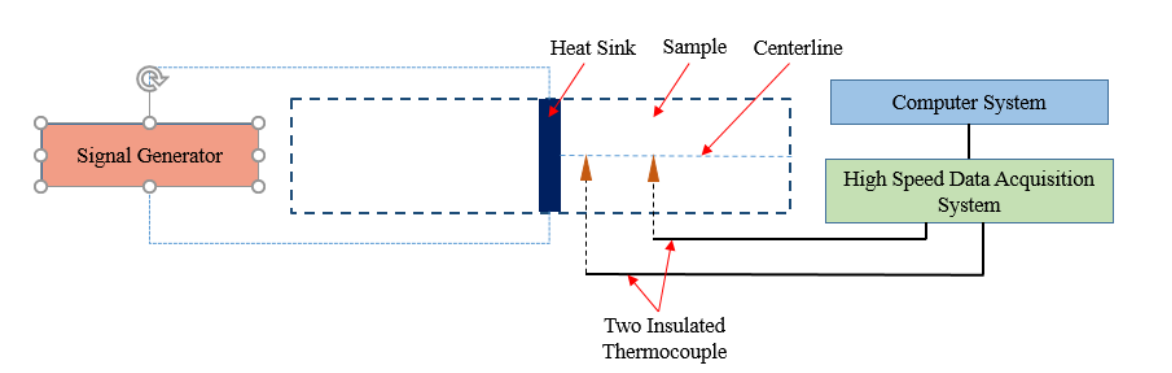

Figure 3.1. Schematic set-up diagram of Angstrom method

If one end of sample is periodically heated, the temperature along the sample varies with the same period but with diminishing amplitude. For our experiment, a periodic heat pulse is applied in the middle of the sample as shown in Figure 4.1. Amplitude decays along the length of the material and experiences a phase shift.

As an advantage of the method, instead of absolute measurements of the temperature, only relative changes in magnitude of temperature as a function of time and position must be recorded.

3.1.1 Theory

One dimensional heat diffusion equation including the effect of heat loss can be written as

$$\frac{\partial^2 T}{\partial x^2} = \frac{1}{\alpha}\frac{\partial T}{\partial t} + m^2 T \quad (3.1)$$

where α^2 is thermal diffusivity[m^2/s], T is the temperature[k], and m is the coefficient of surface heat loss. Although heat loss includes convection ($\sim$T) and radiation ($\sim T^4$), we only use the homogeneous T-linear term $m^2 T$ as an approximation for math convenience.

When a sinusoidal heat wave is applied to the sample, solution of the equation 3.1 can be written in waveform of

$$T(x,t) = A + B(x)e^{iwt} \quad (3.2)$$

Where, i is the unit imaginary, w is angular frequency of the heat wave, and A is a constant, indicative of the baseline temperature for temperature oscillation. One can also set A= 0 for mathematical convenience so that the T can be taken as temperature deviation from the base-line rather than the absolute temperature. The temperature variation induced by the waveform heating has a complex amplitude.

Equation 3.2 turns into

$$T(x,t) = B(x)e^{iwt} \quad (3.3)$$

Substituting eq. 3.3 into eq. 3.1, the second order ordinary differential equation for $B(x)$ gives

$$B_{xx}(x) - \left(\frac{iw}{\alpha} + m^2\right)B_x(x) = 0 \quad (3.4)$$

Where $B_{xx}(x)$ is the second derivative of $B_x(x)$ with respect to x. The general solution of eq. 3.4

$$B(x) = C_1 e^{\beta x} + C_2 e^{-\beta x} \quad (3.5)$$

where, $\beta^2 = m^2 + \frac{iw}{\alpha}$ (3.6)

C_1 & C_2 are constants can be determined by the boundary condition

For a semi-infinite sample, a non-zero, C_1 will render $C_1 e^{\beta x}$ term infinitely large, which has no physical meaning. Thus, under semi-infinite condition solution becomes

$$B(x) = be^{-\beta x} \quad 3.7$$

The complex β is defined as

$$\beta = P + iQ \quad 3.8$$

Eq. 3.6 gives

$$PQ = \frac{w}{2\alpha} \quad 3.9$$

And

$$P^2 + Q^2 = m^2 \quad 3.10$$

Both Eqs. 3.9 and 3.10 are very useful expressions. The product of P and Q, which is not related to heat loss parameter, is used to determine the thermal diffusivity.

According to above equations, temperature variation can be expressed by

$$T(x,t) = be^{-\beta x}e^{iwt} = be^{-Px}e^{i(wt-Qx)} \quad 3.11$$

Measuring the waveform temperature waves at two different positions can give P and Q.

From the ratio of two amplitudes, P is given as,

$$\frac{M}{N} = \frac{be^{-Px_1}}{be^{-Px_2}} = e^{PL} \quad 3.12$$

$$P = \frac{1}{L}\ln\frac{M}{N} \quad 3.13$$

where M and N are temperature amplitude at two different points along the sample, x_1 and x_2, $L = (x_2 - x_1)$ is the distance between two measuring points.

From the phase shift dt between two waveforms, Q is given as

$$wt - Qx_1 = w(t + dt) - Qx_2 \quad 3.14$$

$$Q = \frac{wdt}{L} \quad 3.15$$

Multiplying Eq. 3.13 using Eq. 3.15 and using the *PQ* product relation from 3.9 yields

$$\alpha = \frac{L^2}{2dt \times \ln\frac{M}{N}} \quad 3.16$$

Above expression is used to measure thermal diffusivity.

By plugging Eq. (3.14) and (3.16) into eq. (3.8) for the first harmonic we obtain,

$$\alpha = \frac{k}{\rho C_p} = \frac{L^2}{2dt \times \ln(\frac{M}{N})} \quad 3.17$$

where L is the distance between temperature sensors; dt is the phase difference between two temperature responses, M and N are the amplitudes of the thermal wave measured at the two locations. Finally, thermal conductivity can be derived using

$$k = \rho \alpha C_p \quad 3.18$$

where *k* represents thermal conductivity [81].

3.1.2 Experimental Set up

Thermal conductivity measurement setup is shown in Figure 3.2(a). Preparing samples for in-plane thermal conductivity measurement using the Angstrom method involves embedding a heat source inside the sample and connecting two thermocouples in two different locations near the heat source. A small resistance heater with 1-2 mm width was made in the middle of sample (Figure 3.2 b. A high resistance wire is used for making the heater which has resistance of 80 Ω/ft. Then high thermal conductivity thermal paste is used to cover the heater so that it keeps good contact with the sample. Two thermocouples are attached to the sample at two different locations at distances of 2 and 6 mm from the heater, respectively.

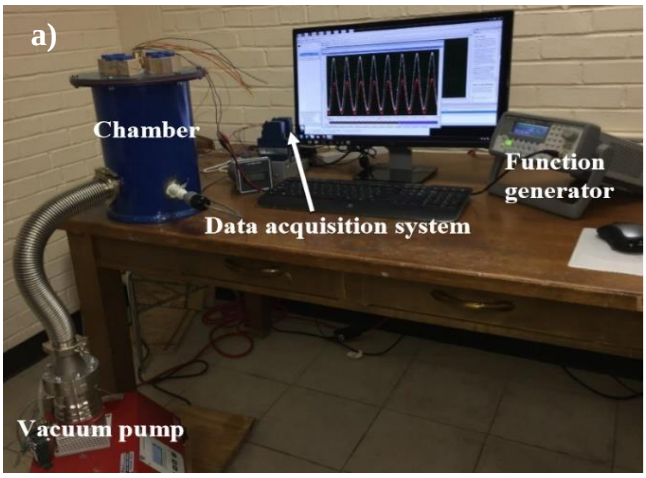

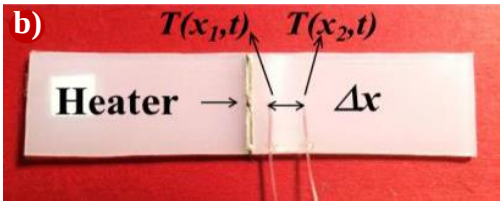

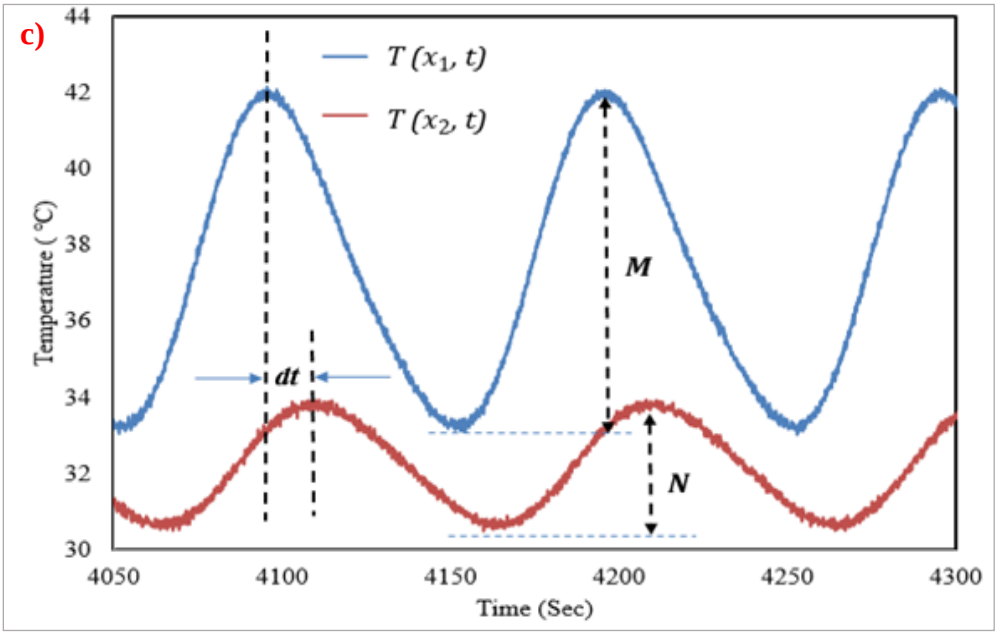

Figure 3.2. a) Thermal diffusivity measurement set-up based on the Angstrom method, b) Prepared sample, c) Temperature vs time profile

A function generator supplies sinusoidal heat pulse to the heater. The sample is placed inside high vacuum while collecting the data from the experiment. A turbo pump is used to evacuate the chamber. Specific heat and density are measured using Pycnometer (AccuPyc 1340V2.0) and Differential Scanning Calorimeter (DSC-Q1000) respectively. Figures 3.3 shows the extracted temperature profiles for PE-GNP with 9wt% graphene at draw ratio 3.

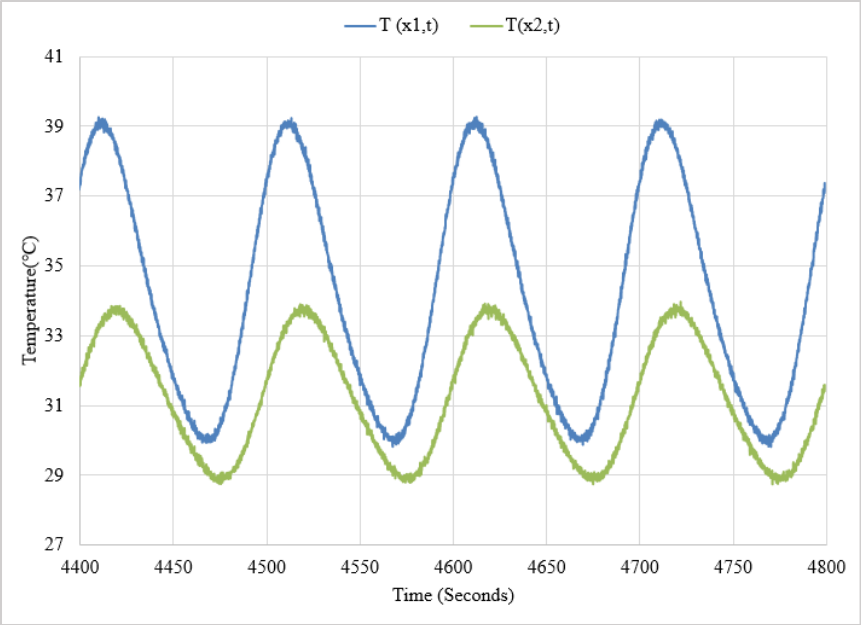

Figure 3.3. Temperature vs Time profile for PE-GNP (9 wt%) at draw ratio 3

Chapter 4: Characterization of Nanoplatelet Alignment Using Confocal Microscopy and ImageJ

Imaging techniques used for characterizing the alignment of dispersed graphene flakes are briefly discussed in this chapter. Laser Scanning Confocal Microscopy (LSCM) [82] is implemented for characterization of alignment of graphene flakes.

4.1 Confocal Microscopy

LSCM is built around a conventional light microscope, and uses a laser rather than a lamp for a light source, sensitive photomultiplier tube detectors (PMTs), and a computer to control the scanning mirrors and to facilitate the collection and display of the images [83]. A confocal microscope creates sharp images of a specimen that would otherwise appear blurred when viewed with a conventional microscope. This is achieved by excluding most of the light from the specimen that is not from the microscope's focal plane. The image has less haze and better contrast than that of a conventional microscope and represents a thin cross-section of the specimen. Point-to-point illumination of the specimen and the pinhole apertures are the key features of modern confocal microscope. Advances in optics and electronics have been incorporated into current designs and provide improvements in speed, image quality, and storage of the generated images [84].

4.2 Principles of Confocal Microscopy

The principle of epifluorescence laser scanning microscope is diagrammatically presented in Figure 4.1. The specimen is excited by coherent light emitted by the laser system (excitation source) which passes through a pinhole aperture that is situated in a conjugate plane (confocal) with a scanning point on the specimen and a second pinhole aperture positioned in front of the detector (a photomultiplier tube). As the laser is reflected by a dichromatic mirror and scanned across the specimen in a defined focal plane, secondary fluorescence emitted from points on the specimen (in the same focal plane) pass

back through the dichromatic mirror and are focused as a confocal point at the detector pinhole aperture. The significant amount of fluorescence emission that occurs at points above and below the objective focal plane is not confocal with the pinhole (termed Out-of-Focus Light Rays in Figure 4.1 and forms extended Airy disks in the aperture plane.

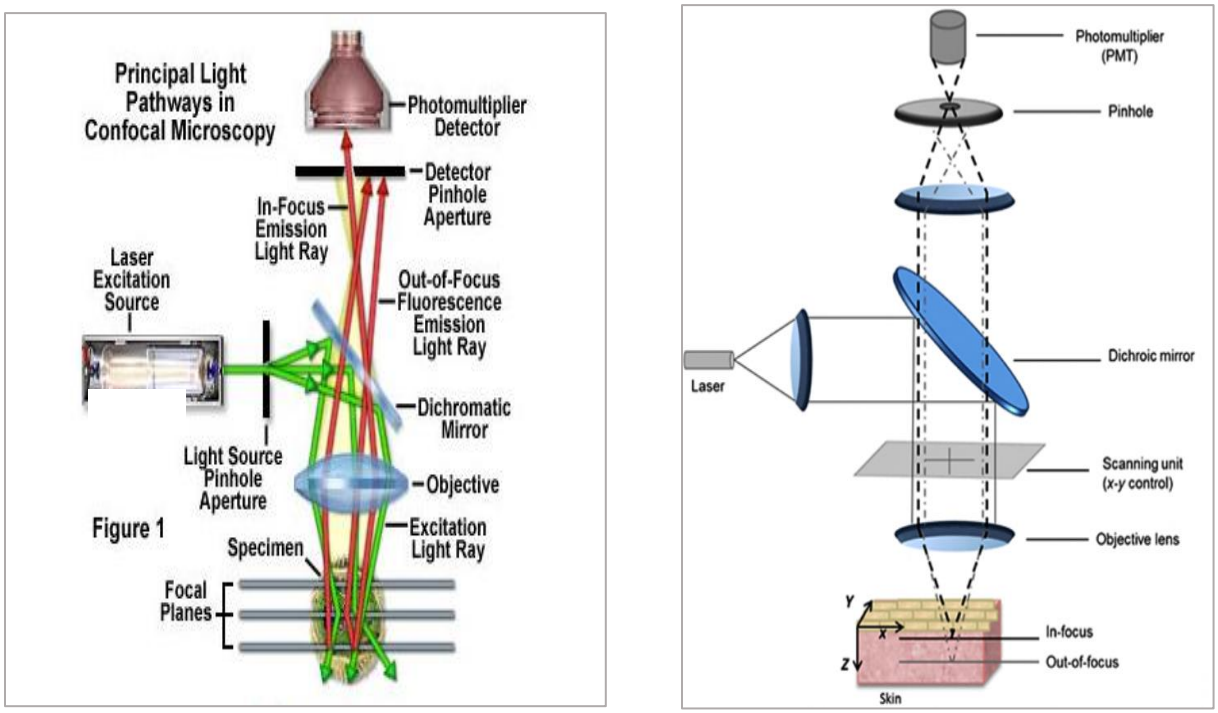

Figure 4.1. Schematic diagram of the optical pathway and principal components in a laser scanning confocal microscope [85, 86]

Because only a small fraction of the out-of-focus fluorescence emission is delivered through the pinhole aperture, most of this extraneous light is not detected by the photomultiplier and does not contribute to the resulting image. Refocusing the objective in a confocal microscope shifts the excitation and emission points on a specimen to a new plane that becomes confocal with the pinhole apertures of the light source and detector.

Laser scanning confocal microscopes employ a pair of pinhole apertures to limit the specimen focal plane to a confined volume approximately a micron in size. This confocal pinhole would block the light, which is emitted from the object region, not in the focal plane. The pinhole is

confocal to the focal point of the specimen. Hence, the light which is emitted from the focal plane of the specimen (in-focal plane) is allowed to pass and rest of the light is eliminated. This would generate a sharp and distinct image. Relatively thick specimens can be imaged in successive volumes by acquiring a series of sections along the optical (z) axis of the microscope. Laser scanning confocal microscopy (LSCM) collects the z-series, a sequence of optical sections from different levels of specimen. Z-series are collected by correlating the movement of the fine focus of the microscope with image collection usually using a computer-controlled stepping motor to move the stage of the microscope by preset distances. By collecting a series of optical sections along the optical axis (Z-axis), one can generate a 3D reconstruction of a volume within an intact specimen with up to 300nm resolution. Scanning a focused laser beam allows the acquisition of digital images with very high resolution since the resolution is determined by the position of the beam rather than the pixel size of the detector[83, 85].

4.3 Characterization of Alignment of Graphene Flakes Using Laser Scanning Confocal Microscopy (LSCM)

Laser Scanning Confocal Microscopy (LSCM) has been used to study the alignment of GnPs. Leica SP8 laser scanning confocal microscope with a 561 nm DPSS laser was used for imaging in this study. The samples have been imaged with a 63x/1.4 oil immersion objective with the pinhole aperture at 0.2 AU and voxel dimensions of 90.2 nm x 90.2 nm x 166.4 nm and to a depth of 11 μm. Figure 4.2 shows LSCM images of GNPs in unstretched PE/GNP (9wt%) nanocomposite sample and same composition sample with different stretch ratios. While GNPs are seen to be randomly oriented in Figure 4.2 a, Figures 4.2 b-e clearly show alignment of GNPs along the stretch direction.

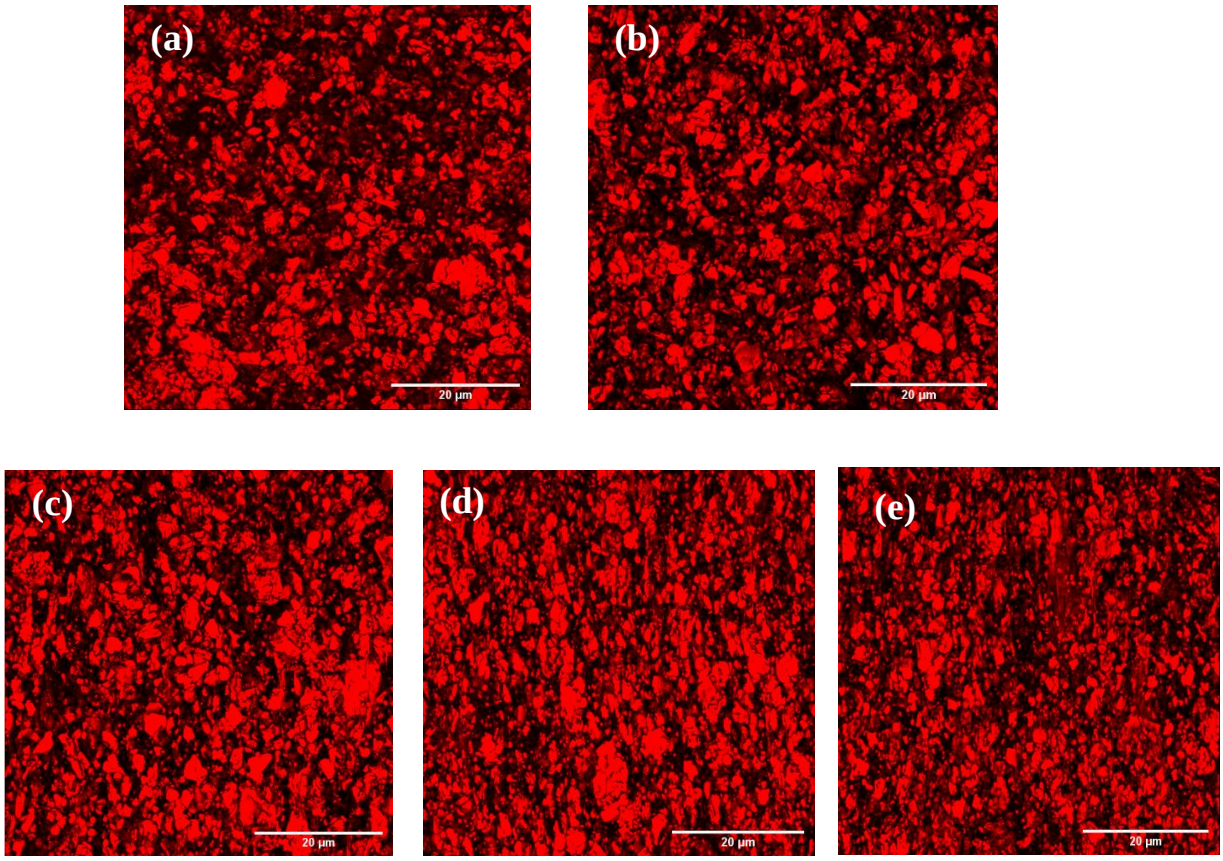

Figure 4.2. Images of PE-GNP composite sample using Laser Scanning Confocal Microscopy for different applied strain, ε, where (a) unstretched sample, $\varepsilon = 0$, and stretched sample (b) $\varepsilon = 1$, (c) $\varepsilon = 2$, (d) $\varepsilon = 3$, (e) $\varepsilon = 4$

4.4 Image Analysis

Using confocal optical sectioning, an image of a section is found from the thick PE-GnP sample. Stacking the z-planes creates a 3D image of the sample. From the 3D image, average angle between GnP and stretching direction is measured using ImageJ software. To find out the angle, all the slices within a certain thickness are used for detecting GnP particles in each image. Using 3D object counter plugin, the number of 3D objects can be detected as shown in figure 4.3. This plugin generates object's map as result. Then 3D ellipsoid fitting plugin is used to fit individual particles into ellipses. After fitting the 3D ellipsoid to objects, this plugin provides a result table with

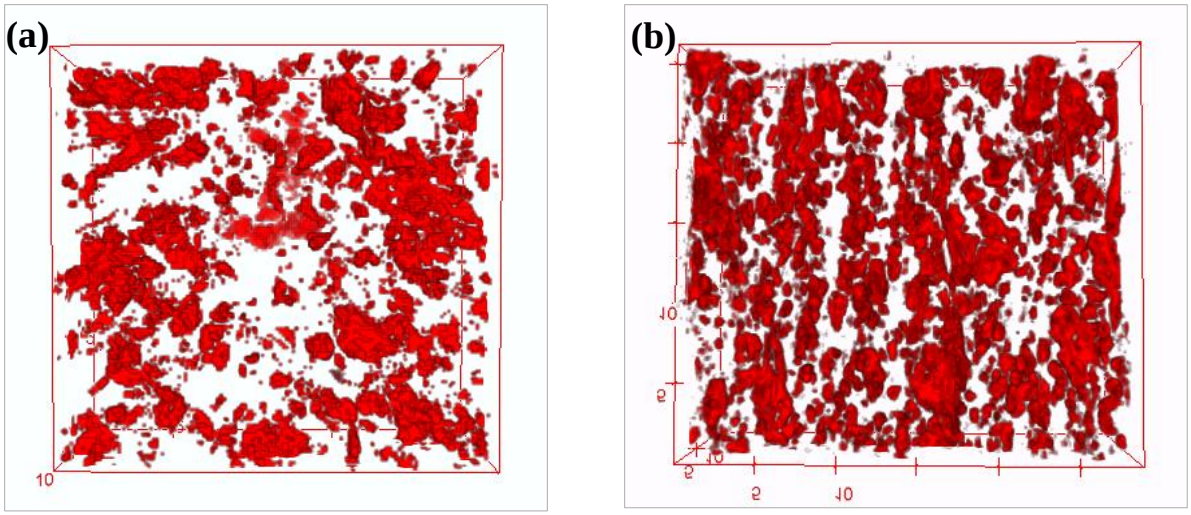

Figure 4.3. 3D view of PE-GnP composites using ImageJ software a) Strain, ε= 0, and b) Strain, ε=4

detailed information for each ellipsoid. From the result table, coordinates of three main elongation axis of 3D ellipsoid can be found. Vector of shortest elongation axis is considered as a normal vector to the ellipsoid.

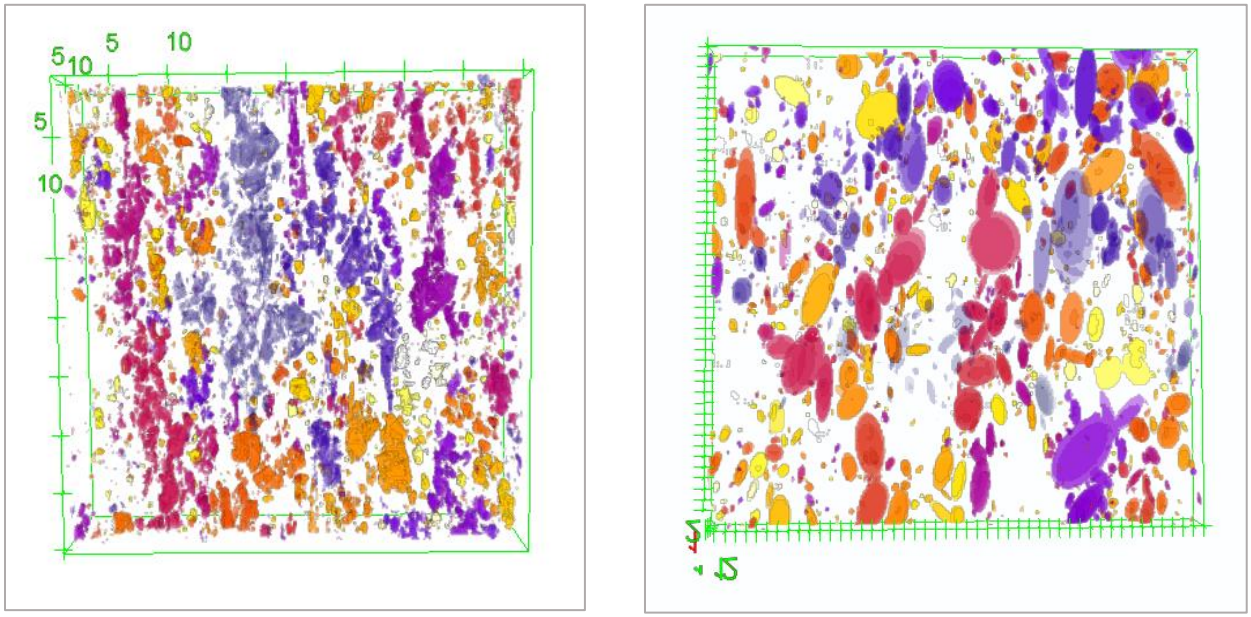

Figure 4.4. ImageJ analysis to find the angle between GnP and stretching direction using a) 3D object counter plugin, and b) 3D object ellipsoid fitting plugin

The direction angle of the normal vector with respect to the stretch direction is calculated using the formula $\theta = \cos^{-1}[x/\sqrt{(x^2 + y^2 + z^2)}]$ where x is the stretching direction of sample. Value of φ can be less or higher than 90°. If $\varphi > 90°$, φ value is subtracted from 180°, then $\varphi' = 180° - \varphi$. The angle between graphene nanoplatelet and alignment direction, $\theta = 90° - \varphi$ or $90° - \varphi'$. Average angle is measured for approximately 3000~4000 GnPs using excel data analysis for each sample. Repetitive calculation was done for different location of different weight percentage PE-GnP composite sample and also for strain range, 0 to 4.

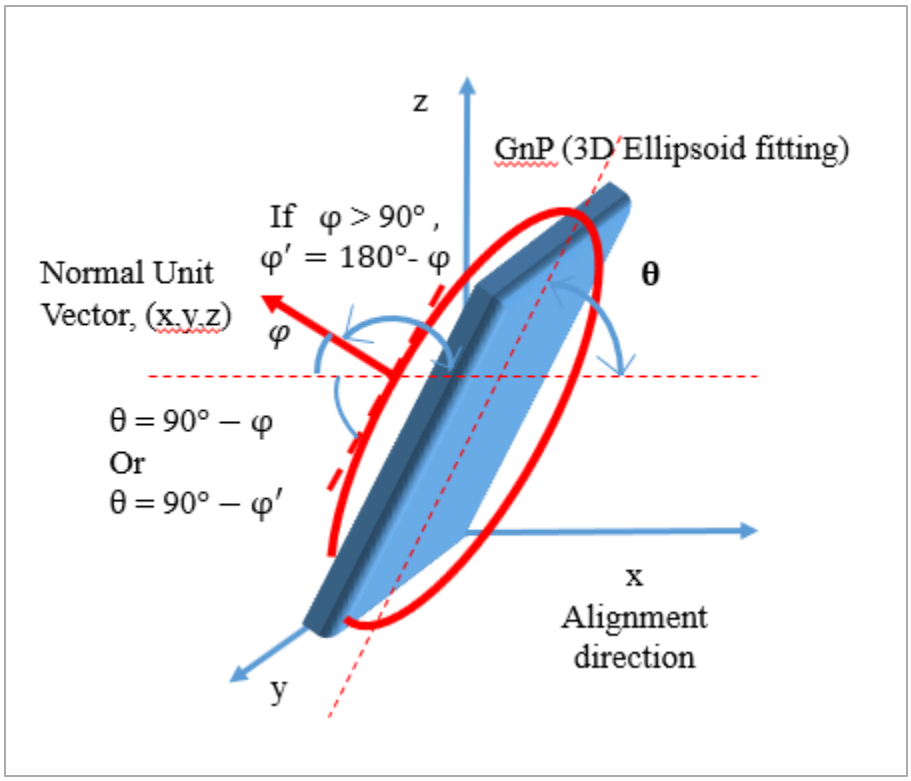

Figure 4.5. Calculation of the angle between GnP and stretching direction

Chapter 5: Result

In this chapter, results obtained from the experimental measurements are presented and compared against theoretical predictions obtained from effective medium theory. Thermal conductivity is derived using thermal diffusivity, specific heat and density obtained from the Angstrom method, differential scanning calorimeter and pycnometer respectively. Table 5.1 displays the specific heat and density of the specimens used for calculating conductivity.

Table 5.1. Specific Heat and density of the material [6]

Sample	Specific Heat [J/g.K]	Density[g/cm^3]
Pure Polyethylene	2.18	0.98
PE/GNP (9 wt%)	2.053	1.038
PE/GNP (13 wt%)	1.994	1.062

From the experimental result it has been observed that the density of PE/GNP samples increases, while the specific heat of PE/GNP specimen decreases with increase in the content of graphene nanoplatelets.

Table 5.2. Thermal Conductivity value of Pure PE and PE/GNP composite

Strain	Thermal Conductivity (W/mK^{-1})		
	Pure PE	PE/GNP (9 wt%)	PE/GNP (13 wt%)
0	0.5	1.23	2.16
1	0.8	2.52	3.88
2	1.5	4.06	4.81
3	2.3	5.03	5.55
4	3.5	5.44	-

Thermal conductivity values obtained from experiments for PE-GNP (9wt%) and PE-GNP (13wt%) aligned composite samples with draw ratios between 1 to 5 are displayed in Table 5.2. Thermal conductivity values for pure PE are also presented here for comparison [6]. Applied strain is represented by σ, where $\sigma = \Delta l / l_0$, l_0 is the initial sample length and Δl is the change in length after stretching.

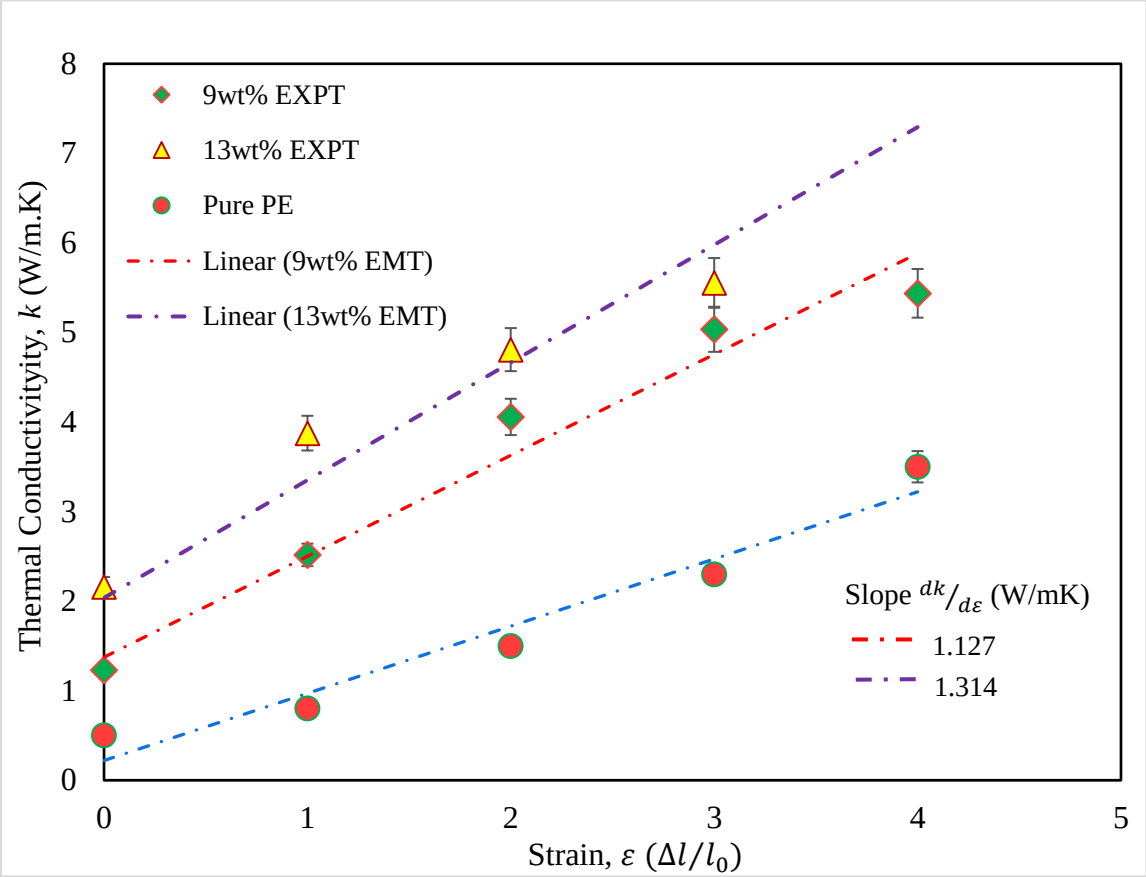

Figure 5.1. Thermal conductivity enhancement of pure PE, PE/GNP (9 wt%) and PE/GNP (13 wt%) as a function of strain and curve fitting with EMT model

Figure 5.1 shows that as the applied strain is increased, there is an increment in thermal conductivity value of the nanocomposite sample due to alignment of PE chain and GNPs.

The thermal conductivity for unoriented pure PE is ~ 0.5 W/mK^{-1}, while for oriented sample the value reached k = 3.5 at an applied strain of, $\varepsilon = 4$. According to the figure 5.1, thermal

conductivity increases with the addition of GNP in the polymer. Along with this, alignment of GNP in the polymer matrix also enhances thermal conductivity. For 9 weight% GNP in the composite, *k* value of 1.23 W/mK^{-1} is achieved with randomly oriented GNPs. For 400% strain, approximately 1000% increment in the thermal conductivity value (*k*= 5.44 W/ mK^{-1}) is achieved for 9 weight% PE-GNP sample compared to the unoriented pure PE *k* value. Higher amount of filler content in the polymer matrix enhances the thermal conductivity value. For 13wt% aligned PE-GNP composite, 1100% increment in *k* value has been found for the highest applied strain, $\varepsilon = 3$ in comparison to pure polyethylene.

Above measurements clearly show that graphene nanoplatelets play an effective role in increasing the thermal conductivity of nanocomposite in both the randomly oriented and aligned configuration.

5.1 Comparison with effective medium theory

Effects contributing to an interfacial thermal barrier are characterized by an average interfacial thermal resistance, R, between the polymer matrix and GNPs for theoretical prediction. The inclusive effect of R is to decrease the thermal conductivity of the composites, and this kind of reduction can be noticeable for different nanofillers [73].

According to Nan effective medium theory, effective thermal conductivity of aligned PE/GNP composite can be predicted by including the effect of geometrical factors, nanoplatelet alignment and interfacial thermal resistance [87, 88]. Geometrical parameters, L_{ii} are computed based on the aspect ratio, *p* of the graphene nanoparticle, where, aspect ratio is the ratio of the thickness(t) to the lateral dimension (L) of the nanoplatelet. For oblate inclusion, $p = \frac{t}{L} < 1$

$$L_{11} = L_{22} = \frac{p^2}{2(p^2-1)} + \frac{p}{2(1-p^2)^{3/2}} \cos^{-1} p \quad (5.1)$$

$$L_{33} = 1 - 2L_{11} \quad (5.2)$$

The effective thermal conductivities of the nanoplatelet along in-plane and out-of-plane are respectively,

$$K_{11}^c = K_{22}^c = \frac{k_{in}}{1+\gamma L_{11} k_{in}/k_m} \quad (5.3)$$

$$K_{33}^c = \frac{k_{out}}{1+\gamma L_{33} k_{out}/k_m} \quad (5.4)$$

$$\gamma = (1 + 2p)\alpha \quad (5.5)$$

Dimensionless parameter, $\alpha = \frac{R k_m}{t}$ (5.6)

where, k_{in} & k_{out} represent the in-plane and out-of-plane thermal conductivity of graphene nanoparticle respectively, k_m is the thermal conductivity of polymer matrix and R represents interfacial thermal resistance between polymer and graphene.

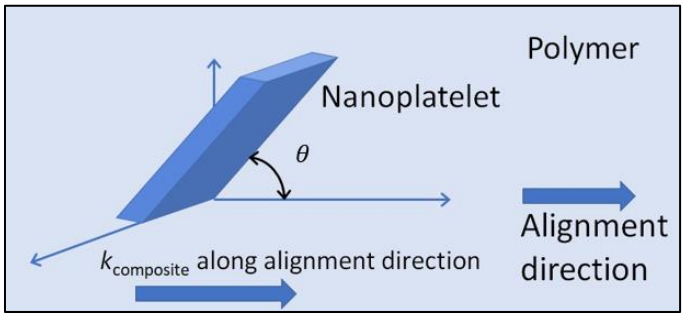

Figure 5.2. Orientation of GNP with the stretching direction

Then, taking the alignment effect of GNP, the effective thermal conductivity of composite material along the alignment direction can be calculated using following equation where θ represents the orientation angle between GNP and alignment direction.

$$K_{effective}^{alignment} = k_m \frac{2+f[\beta_{11}(1-L_{11})(1+<\cos^2\theta>)+\beta_{33}(1-L_{33})(1-<\cos^2\theta>)]}{2+f[\beta_{11}L_{11}(1+<\cos^2\theta>)+\beta_{33}L_{33}(1-<\cos^2\theta>)]} \quad 5.7$$

$$\text{here, } \beta_{ii} = \frac{K_{ii}^c - k_m}{k_m + L_{ii}(K_{ii}^c - k_m)} \quad 5.8$$

The predicted values are shown as dashed lines in Fig. 5.1. Different parameters involved in the prediction are provided in Table 5.3.

Table 5.3. Specification of materials used to calculate effective thermal conductivity

Lateral Dimension of Graphene nanoplatelet (L)	5μm
Thickness of nanoplatelets (t)	60 nm
Interface thermal resistance(R)	$6 \times 10^{-8} \text{m}^2\text{K/W}$ [89]
k-graphene, in -plane (k_{in})	1000 W/ mK^{-1}
k-graphene, out-of-plane (k_{out})	10 W/ mK^{-1}
Filler Volume ratio (f)	0.037 & 0.057

Value of $\text{Cos}^2\,\theta$ used to calculate effective thermal conductivity was derived from confocal microscopy measurements. Increment in value of $\cos^2\theta$ indicates improvement in GNP alignment. Measured values of $\text{Cos}^2\,\theta$ for different applied strains for 9wt% PE-GnP composite are presented in Table 5.4.

Table 5.4. Measured Angle value for 9wt% PE-GnP composite from ImageJ analysis

Draw ratio	Angle (θ)	$\cos^2\theta$
1	39.03	0.603
2	32.41	0.713
3	26.98	0.794
4	25.68	0.812
5	24.46	0.829

Figure 5.1 displays good agreement between theoretical *k* values and experimental measurements. However, a limitation of the model involves assumption of isotropic base matrix thermal conductivity. In this work, the thermal conductivity of the polymer matrix along the alignment direction was taken to be the isotropic value. Clearly, this overestimates the average polymer matrix thermal conductivity. The predicted values thus represent an upper bound of the thermal conductivity of aligned composites.

Chapter 6: Conclusion and Remarks

The effect of alignment on thermal conductivity enhancement of graphene (PE/GNP) nanoplatelets has been experimentally studied. PE-GNP nanocomposites were fabricated using melt-mixing method and compression molding. Alignment effect was gained through mechanical stretching. Laser Scanning Confocal Microscopy (LSCM) was used to quantitatively study the alignment of graphene nanoplatelets. In-plane thermal conductivity of composites was measured using Angstrom method. PE-GNP composites with 9wt% and 13wt% were prepared and stretched to understand the effect of alignment and nanofiller content. Experimental analysis clearly shows the effect of graphene nanoplatelets aligned in the nanocomposites along with the effect of increase in filler amount.

It is evident that simultaneous alignment of polymer chains and dispersed GNPs can provide high thermal conductivity values. The thermal conductivity of nanocomposites increased to 5.0 W/mK (9 wt%) and 5.55W/mK (13 wt%) for the same draw ratio. Thermal conductivity enhancement in pure PE sample is due to alignment of PE chains alone, while *k* enhancement in the nanocomposite is due to alignment of both PE chains and GNPs. These experimental values agree with theoretical prediction of thermal conductivity values found from effective medium theory.

References

1. A.L. Moore, L. Shi, *Emerging challenges and materials for thermal management of electronics.* Materials today, 2014. **17**(4): p. 163-174.
2. H. Chen, V.V. Ginzburg, J. Yang, Y. Yang, W. Liu, Y. Huang, L. Du, B. Chen, *Thermal conductivity of polymer-based composites: Fundamentals and applications.* Progress in Polymer Science, 2016. **59**: p. 41-85.
3. C. T'Joen, Y. Park, Q. Wang, A. Sommers, X. Han, A. Jacobi, *A review on polymer heat exchangers for HVAC&R applications.* International journal of refrigeration, 2009. **32**(5): p. 763-779.
4. D. Bigg, G. Stickford, S. Talbert, *Applications of polymeric materials for condensing heat exchangers.* Polymer Engineering & Science, 1989. **29**(16): p. 1111-1116.
5. P. Luckow, A. Bar-Cohen, P. Rodgers, J. Cevallos, *Energy efficient polymers for gas-liquid heat exchangers.* Journal of Energy Resources Technology, 2010. **132**(2): p. 021001.
6. M. Saeidi-Javash, *Effect of Alignment on Thermal Conductivity Enhancement of Polyethylene/Graphene Nanoplatelet Composite Materials.* 2017.
7. X. Chen, Y. Su, D. Reay, S. Riffat, *Recent research developments in polymer heat exchangers–A review.* Renewable and Sustainable Energy Reviews, 2016. **60**: p. 1367-1386.
8. E. Kolasińska, P. Kolasiński, *A review on electroactive polymers for waste heat recovery.* Materials, 2016. **9**(6): p. 485.
9. C. Dreiser, L. Krätz, H. Bart. *Polymer film heat exchanger for seawater desalination: Prevention and cleaning of fouling deposits*. in *Proceedings of International Conference on Heat Exchanger Fouling and Cleaning X*. 2013.

10. W. Liu, J. Davidson, S. Mantell, *Thermal analysis of polymer heat exchangers for solar water heating: a case study.* TRANSACTIONS-AMERICAN SOCIETY OF MECHANICAL ENGINEERS JOURNAL OF SOLAR ENERGY ENGINEERING, 2000. **122**(2): p. 84-91.

11. S. Mallik, N. Ekere, C. Best, R. Bhatti, *Investigation of thermal management materials for automotive electronic control units.* Applied Thermal Engineering, 2011. **31**(2-3): p. 355-362.

12. J. Garg, *Relative effect of edge versus basal plane functionalization on graphene/polymer interfacial thermal conductance-Role of in-plane phonons.* Applied Physics Letters, 2017. **110**(9): p. 093112.

13. X. Lu, G. Xu, *Thermally conductive polymer composites for electronic packaging.* Journal of applied polymer science, 1997. **65**(13): p. 2733-2738.

14. P. Procter, J. Solc, *Improved thermal conductivity in microelectronic encapsulants.* IEEE Transactions on Components, Hybrids, and Manufacturing Technology, 1991. **14**(4): p. 708-713.

15. F. Luzi, L. Torre, J.M. Kenny, D. Puglia, *Bio-and fossil-based polymeric blends and nanocomposites for packaging: Structure–property relationship.* Materials, 2019. **12**(3): p. 471.

16. Y. Pan, M. Farmahini-Farahani, P. O'Hearn, H. Xiao, H. Ocampo, *An overview of bio-based polymers for packaging materials.* Journal of Bioresources and Bioproducts, 2016. **1**(3): p. 106-113.

17. M. Hu, D. Yu, J. Wei, *Thermal conductivity determination of small polymer samples by differential scanning calorimetry.* Polymer testing, 2007. **26**(3): p. 333-337.

18. Y. Agari, A. Ueda, Y. Omura, S. Nagai, *Thermal diffusivity and conductivity of PMMA/PC blends.* Polymer, 1997. **38**(4): p. 801-807.

19. H. Ebadi-Dehaghani, M. Nazempour, *Thermal conductivity of nanoparticles filled polymers*, in *Smart nanoparticles technology*. 2012, IntechOpen.

20. T. Tanaka, G. Montanari, R. Mulhaupt, *Polymer nanocomposites as dielectrics and electrical insulation-perspectives for processing technologies, material characterization and future applications.* IEEE transactions on Dielectrics and Electrical Insulation, 2004. **11**(5): p. 763-784.

21. J. Hu, Y. Huang, Y. Yao, G. Pan, J. Sun, X. Zeng, R. Sun, J.-B. Xu, B. Song, C.-P. Wong, *Polymer composite with improved thermal conductivity by constructing a hierarchically ordered three-dimensional interconnected network of BN.* ACS applied materials & interfaces, 2017. **9**(15): p. 13544-13553.

22. H.S. Lim, J.W. Oh, S.Y. Kim, M.-J. Yoo, S.-D. Park, W.S. Lee, *Anisotropically alignable magnetic boron nitride platelets decorated with iron oxide nanoparticles.* Chemistry of Materials, 2013. **25**(16): p. 3315-3319.

23. A. Yu, P. Ramesh, X. Sun, E. Bekyarova, M.E. Itkis, R.C. Haddon, *Enhanced thermal conductivity in a hybrid graphite nanoplatelet–carbon nanotube filler for epoxy composites.* Advanced Materials, 2008. **20**(24): p. 4740-4744.

24. A. Moisala, Q. Li, I. Kinloch, A. Windle, *Thermal and electrical conductivity of single- and multi-walled carbon nanotube-epoxy composites.* Composites science and technology, 2006. **66**(10): p. 1285-1288.

25. S.-Y. Yang, C.-C.M. Ma, C.-C. Teng, Y.-W. Huang, S.-H. Liao, Y.-L. Huang, H.-W. Tien, T.-M. Lee, K.-C. Chiou, *Effect of functionalized carbon nanotubes on the thermal conductivity of epoxy composites.* Carbon, 2010. **48**(3): p. 592-603.

26. Y.S. Song, J.R. Youn, *Evaluation of effective thermal conductivity for carbon nanotube/polymer composites using control volume finite element method.* Carbon, 2006. **44**(4): p. 710-717.

27. B. Li, R. Li, Y. Xie, *Properties and effect of preparation method of thermally conductive polypropylene/aluminum oxide composite.* Journal of materials science, 2017. **52**(5): p. 2524-2533.

28. S. Kidalov, F. Shakhov, *Thermal conductivity of diamond composites.* Materials, 2009. **2**(4): p. 2467-2495.

29. Z. Han, A. Fina, *Thermal conductivity of carbon nanotubes and their polymer nanocomposites: A review.* Progress in polymer science, 2011. **36**(7): p. 914-944.

30. Y.P. Mamunya, V. Davydenko, P. Pissis, E. Lebedev, *Electrical and thermal conductivity of polymers filled with metal powders.* European polymer journal, 2002. **38**(9): p. 1887-1897.

31. Y. Chen, J. Gao, Q. Yan, X. Hou, S. Shu, M. Wu, N. Jiang, X. Li, J.-B. Xu, C.-T. Lin, *Advances in graphene-based polymer composites with high thermal conductivity.* Veruscript Functional Nanomaterials, 2018. **2**: p. OOSB06.

32. A.A. Balandin, S. Ghosh, W. Bao, I. Calizo, D. Teweldebrhan, F. Miao, C.N. Lau, *Superior thermal conductivity of single-layer graphene.* Nano letters, 2008. **8**(3): p. 902-907.

33. G. Fugallo, A. Cepellotti, L. Paulatto, M. Lazzeri, N. Marzari, F. Mauri, *Thermal conductivity of graphene and graphite: collective excitations and mean free paths.* Nano letters, 2014. **14**(11): p. 6109-6114.

34. S. Ghosh, W. Bao, D.L. Nika, S. Subrina, E.P. Pokatilov, C.N. Lau, A.A. Balandin, *Dimensional crossover of thermal transport in few-layer graphene.* Nature materials, 2010. **9**(7): p. 555.

35. C. Huang, X. Qian, R. Yang, *Thermal conductivity of polymers and polymer nanocomposites.* Materials Science and Engineering: R: Reports, 2018. **132**: p. 1-22.

36. T. Zhang, T. Luo, *Morphology-influenced thermal conductivity of polyethylene single chains and crystalline fibers.* Journal of Applied Physics, 2012. **112**(9): p. 094304.

37. J. Liu, R. Yang, *Tuning the thermal conductivity of polymers with mechanical strains.* Physical Review B, 2010. **81**(17): p. 174122.

38. T. Luo, G. Chen, *Nanoscale heat transfer–from computation to experiment.* Physical Chemistry Chemical Physics, 2013. **15**(10): p. 3389-3412.

39. O.M. Istrate, K.R. Paton, U. Khan, A. O'Neill, A.P. Bell, J.N. Coleman, *Reinforcement in melt-processed polymer–graphene composites at extremely low graphene loading level.* Carbon, 2014. **78**: p. 243-249.

40. Y. Zhan, J. Wu, H. Xia, N. Yan, G. Fei, G. Yuan, *Dispersion and exfoliation of graphene in rubber by an ultrasonically-assisted latex mixing and in situ reduction process.* Macromolecular Materials and Engineering, 2011. **296**(7): p. 590-602.

41. B. Shen, W. Zhai, C. Chen, D. Lu, J. Wang, W. Zheng, *Melt blending in situ enhances the interaction between polystyrene and graphene through π–π stacking.* ACS applied materials & interfaces, 2011. **3**(8): p. 3103-3109.

42. Q. Wang, J. Dai, W. Li, Z. Wei, J. Jiang, *The effects of CNT alignment on electrical conductivity and mechanical properties of SWNT/epoxy nanocomposites.* Composites science and technology, 2008. **68**(7-8): p. 1644-1648.

43. M. Monti, M. Natali, L. Torre, J.M. Kenny, *The alignment of single walled carbon nanotubes in an epoxy resin by applying a DC electric field.* Carbon, 2012. **50**(7): p. 2453-2464.

44. C. Ma, W. Zhang, Y. Zhu, L. Ji, R. Zhang, N. Koratkar, J. Liang, *Alignment and dispersion of functionalized carbon nanotubes in polymer composites induced by an electric field.* Carbon, 2008. **46**(4): p. 706-710.

45. T. Prasse, J.-Y. Cavaille, W. Bauhofer, *Electric anisotropy of carbon nanofibre/epoxy resin composites due to electric field induced alignment.* Composites Science and Technology, 2003. **63**(13): p. 1835-1841.

46. R.B. Ladani, S. Wu, A.J. Kinloch, K. Ghorbani, J. Zhang, A.P. Mouritz, C.H. Wang, *Improving the toughness and electrical conductivity of epoxy nanocomposites by using aligned carbon nanofibres.* Composites Science and Technology, 2015. **117**: p. 146-158.

47. C.-S. Lim, A.J. Rodriguez, M.E. Guzman, J.D. Schaefer, B. Minaie, *Processing and properties of polymer composites containing aligned functionalized carbon nanofibers.* Carbon, 2011. **49**(6): p. 1873-1883.

48. M.-K. Schwarz, W. Bauhofer, K. Schulte, *Alternating electric field induced agglomeration of carbon black filled resins.* Polymer, 2002. **43**(10): p. 3079-3082.

49. W. Jiao, M. Shioya, R. Wang, F. Yang, L. Hao, Y. Niu, W. Liu, L. Zheng, F. Yuan, L. Wan, *Improving the gas barrier properties of Fe3O4/graphite nanoplatelet reinforced*

nanocomposites by a low magnetic field induced alignment. Composites Science and Technology, 2014. **99**: p. 124-130.

50. S. Wu, R.B. Ladani, J. Zhang, A.J. Kinloch, Z. Zhao, J. Ma, X. Zhang, A.P. Mouritz, K. Ghorbani, C.H. Wang, *Epoxy nanocomposites containing magnetite-carbon nanofibers aligned using a weak magnetic field.* Polymer, 2015. **68**: p. 25-34.

51. H. Yan, Y. Tang, W. Long, Y. Li, *Enhanced thermal conductivity in polymer composites with aligned graphene nanosheets.* Journal of materials science, 2014. **49**(15): p. 5256-5264.

52. S.L. Aggarwal, G.P. Tilley, O.J. Sweeting, *Changes in orientation of crystallites during stretching and relaxation of polyethylene films.* Journal of Polymer Science, 1961. **51**(156): p. 551-568.

53. G. Vancso, D. Snétivy, I. Tomka, *Structural changes during polystyrene orientation: A study of optical birefringence and wide angle X-ray scattering.* Journal of applied polymer science, 1991. **42**(5): p. 1351-1359.

54. S.-H. Yao, J.-K. Yuan, T. Zhou, Z.-M. Dang, J. Bai, *Stretch-modulated carbon nanotube alignment in ferroelectric polymer composites: characterization of the orientation state and its influence on the dielectric properties.* The Journal of Physical Chemistry C, 2011. **115**(40): p. 20011-20017.

55. S. Ahir, Y. Huang, E. Terentjev, *Polymers with aligned carbon nanotubes: Active composite materials.* Polymer, 2008. **49**(18): p. 3841-3854.

56. S. Shen, A. Henry, J. Tong, R. Zheng, G. Chen, *Polyethylene nanofibres with very high thermal conductivities.* Nature nanotechnology, 2010. **5**(4): p. 251.

57. C. Choy, *Thermal conductivity of polymers.* Polymer, 1977. **18**(10): p. 984-1004.

58. C. Choy, F. Chen, W. Luk, *Thermal conductivity of oriented crystalline polymers.* Journal of Polymer Science: Polymer Physics Edition, 1980. **18**(6): p. 1187-1207.

59. C. Choy, Y. Wong, G. Yang, T. Kanamoto, *Elastic modulus and thermal conductivity of ultradrawn polyethylene.* Journal of Polymer Science Part B: Polymer Physics, 1999. **37**(23): p. 3359-3367.

60. M. Saeidijavash, J. Garg, B. Grady, B. Smith, Z. Li, R.J. Young, F. Tarannum, N.B. Bekri, *High thermal conductivity through simultaneously aligned polyethylene lamellae and graphene nanoplatelets.* Nanoscale, 2017. **9**(35): p. 12867-12873.

61. A.M. Marconnet, N. Yamamoto, M.A. Panzer, B.L. Wardle, K.E. Goodson, *Thermal conduction in aligned carbon nanotube–polymer nanocomposites with high packing density.* ACS nano, 2011. **5**(6): p. 4818-4825.

62. S. Sihn, S. Ganguli, A.K. Roy, L. Qu, L. Dai, *Enhancement of through-thickness thermal conductivity in adhesively bonded joints using aligned carbon nanotubes.* Composites Science and Technology, 2008. **68**(3-4): p. 658-665.

63. N. Song, D. Jiao, P. Ding, S. Cui, S. Tang, L. Shi, *Anisotropic thermally conductive flexible films based on nanofibrillated cellulose and aligned graphene nanosheets.* Journal of Materials Chemistry C, 2016. **4**(2): p. 305-314.

64. Y. Guo, Y. Chen, E. Wang, M. Cakmak, *Roll-to-Roll Continuous Manufacturing Multifunctional Nanocomposites by Electric-Field-Assisted "Z" Direction Alignment of Graphite Flakes in Poly (dimethylsiloxane).* ACS applied materials & interfaces, 2016. **9**(1): p. 919-929.

65. S. Park, R.S. Ruoff, *Chemical methods for the production of graphenes.* Nature nanotechnology, 2009. **4**(4): p. 217.

66. M.C. Lemme. *Current status of graphene transistors*. in *Solid State Phenomena*. 2010. Trans Tech Publ.

67. K.S. Novoselov, A. Geim, *The rise of graphene.* Nat. Mater, 2007. **6**(3): p. 183-191.

68. A.M. Maharramov, K.T. Mahmudov, M.N. Kopylovich, A.J. Pombeiro, *Non-covalent interactions in the synthesis and design of new compounds*. 2016: Wiley Online Library.

69. E. Pop, V. Varshney, A.K. Roy, *Thermal properties of graphene: Fundamentals and applications.* MRS bulletin, 2012. **37**(12): p. 1273-1281.

70. D. Nika, E. Pokatilov, A. Askerov, A. Balandin, *Phonon thermal conduction in graphene: Role of Umklapp and edge roughness scattering.* Physical Review B, 2009. **79**(15): p. 155413.

71. B.D. Kong, S. Paul, M.B. Nardelli, K.W. Kim, *First-principles analysis of lattice thermal conductivity in monolayer and bilayer graphene.* Physical Review B, 2009. **80**(3): p. 033406.

72. A. Balandin, S. Ghosh, W. Bao, I. Calizo, D. Teweldebrhan, F. Miao, C. Lau, *Extremely high thermal conductivity of graphene: experimental study.* arXiv preprint arXiv:0802.1367, 2008.

73. A.A. Balandin, *Thermal properties of graphene and nanostructured carbon materials.* Nature materials, 2011. **10**(8): p. 569.

74. S. Ghosh, I. Calizo, D. Teweldebrhan, E. Pokatilov, D. Nika, *aa Balandin, W. Bao, F. Miao, and CN Lau,"Extremely high thermal conductivity of graphene: Prospects for thermal management applications in nanoelectronic circuits,".* Appl. Phys. Lett, 2008. **92**(15): p. 15-17.

75. M. Mehrali, S.T. Latibari, M. Mehrali, T.M.I. Mahlia, H.S.C. Metselaar, M.S. Naghavi, E. Sadeghinezhad, A.R. Akhiani, *Preparation and characterization of palmitic acid/graphene nanoplatelets composite with remarkable thermal conductivity as a novel shape-stabilized phase change material.* Applied Thermal Engineering, 2013. **61**(2): p. 633-640.

76. M. Mehrali, S.T. Latibari, M. Mehrali, H.S.C. Metselaar, M. Silakhori, *Shape-stabilized phase change materials with high thermal conductivity based on paraffin/graphene oxide composite.* Energy conversion and management, 2013. **67**: p. 275-282.

77. R.F. Brandenburg, C.M. Lepienski, D. Becker, L.A.F. Coelho, *Influence of mixing methods on the properties of high density polyethylene nanocomposites with different carbon nanoparticles.* Matéria (Rio de Janeiro), 2017. **22**(4).

78. J.E. Parrott, A.D. Stuckes, *Thermal conductivity of solids.* 1975.

79. W. Parker, R. Jenkins, C. Butler, G. Abbott, *Flash method of determining thermal diffusivity, heat capacity, and thermal conductivity.* Journal of applied physics, 1961. **32**(9): p. 1679-1684.

80. G. Bocchini, G. Bovesecchi, P. Coppa, S. Corasaniti, R. Montanari, A. Varone, *Thermal diffusivity of sintered steels with flash method at ambient temperature.* International Journal of Thermophysics, 2016. **37**(4): p. 38.

81. Y. Zhu, *Heat-loss modified Angstrom method for simultaneous measurements of thermal diffusivity and conductivity of graphite sheets: The origins of heat loss in Angstrom method.* International Journal of Heat and Mass Transfer, 2016. **92**: p. 784-791.

82. D. Semwogerere, E.R. Weeks, *Confocal microscopy.* Encyclopedia of biomaterials and biomedical engineering, 2005. **23**: p. 1-10.

83. S.W. Paddock, *Principles and practices of laser scanning confocal microscopy.* Molecular biotechnology, 2000. **16**(2): p. 127-149.

84. T. Wilson, A. Carlini, *Three-dimensional imaging in confocal imaging systems with finite sized detectors.* Journal of Microscopy, 1988. **149**(1): p. 51-66.

85. N.S. Claxton, T.J. Fellers, M.W. Davidson, *Laser scanning confocal microscopy.* Department of Optical Microscopy and Digital Imaging, Florida State University, Tallahassee, http://www. olympusconfocal. com/theory/LSCMIntro. pdf, 2006.

86. F.b.C. Rossetti, L.v.V. Depieri, M. Bentley, *Confocal laser scanning microscopy as a tool for the investigation of skin drug delivery systems and diagnosis of skin disorders.* Confocal laser microscopy-principles and applications in medicine, biology, and the food sciences. InTech, Croatia, 2013: p. 99-140.

87. C.W. Nan, *Effective-medium theory of piezoelectric composites.* Journal of applied physics, 1994. **76**(2): p. 1155-1163.

88. C.-W. Nan, R. Birringer, D.R. Clarke, H. Gleiter, *Effective thermal conductivity of particulate composites with interfacial thermal resistance.* Journal of Applied Physics, 1997. **81**(10): p. 6692-6699.

89. S.T. Huxtable, D.G. Cahill, S. Shenogin, L. Xue, R. Ozisik, P. Barone, M. Usrey, M.S. Strano, G. Siddons, M. Shim, *Interfacial heat flow in carbon nanotube suspensions.* Nature materials, 2003. **2**(11): p. 731.